



ELSEVIER

Contents lists available at ScienceDirect

## Comptes Rendus Biologies

www.sciencedirect.com



Neurosciences / Neurosciences

## Mathematical modeling of energy metabolism and hemodynamics of WHO grade II gliomas using in vivo MR data

*Modélisation mathématique du métabolisme et de l'hémodynamique des gliomes de grade II OMS utilisant les données de la résonance magnétique in vivo*

Rémy Guillevin<sup>a,\*</sup>, Carole Menuel<sup>a</sup>, Jean-Noël Vallée<sup>b</sup>, Jean-Pierre François<sup>c</sup>, Laurent Capelle<sup>a</sup>, Christophe Habas<sup>d</sup>, Giovanni De Marco<sup>e</sup>, Jacques Chiras<sup>a</sup>, Robert Costalat<sup>f,g</sup>

<sup>a</sup> Inserm U678, Functional Imaging Laboratory, Department of Neuroradiology, Pitié-Salpêtrière Hospital, UPMC Univ Paris 06, 47–83, boulevard de l'Hôpital, 75651 Paris cedex 13, France

<sup>b</sup> Department of Neuroradiology, Amiens University Medical Center, University of Picardie–Jules-Vernes, chemin du Thil, 80025 Amiens, France

<sup>c</sup> UMR 7598, CNRS, laboratoire J.-L.-Lions, université Pierre-et-Marie-Curie Paris-6, boîte courrier 187, 75252 Paris cedex 05, France

<sup>d</sup> Department of Neuroradiology, XV-XX Hospital, 28, rue de Charenton, 75012 Paris, France

<sup>e</sup> Laboratoire contrôle moteur et mouvement, UFR STAPS, Paris X, 200, avenue de la République, 92001 Nanterre, France

<sup>f</sup> UPMC, UMI 209, UMMISCO, University of Paris-6, 75005 Paris, France

<sup>g</sup> IRD, UMI 209, UMMISCO, 93143 Bondy cedex, France

## ARTICLE INFO

## Article history:

Received 5 August 2010

Accepted after revision 3 November 2010

Available online 28 December 2010

## Keywords:

In vivo magnetic resonance

Multinuclear spectroscopy

Perfusion imaging

Low-grade glioma

Metabolism

Mathematical modeling

## Mots clés :

Résonance magnétique in vivo

Spectroscopie multinucléaire

Imagerie de perfusion

Gliome de bas grade

Métabolisme

Modélisation mathématique

## ABSTRACT

Therapeutic management of low-grade gliomas (LGG) is a challenge because they have undergone anaplastic transformation with variable delay. Today, only progressive volume growth on successive MRI allows an in vivo monitoring of this evolution. On the other hand, multinuclear spectroscopy and perfusion available during MRI may also provide assessment of metabolic changes underlying morphological modifications. To overcome this drawback, we developed a mathematical model of the metabolism and the hemodynamic of gliomas, based on a physiological model previously published, and including the MR parameters. This allows us to suggest that some specific profiles of metabolic and hemodynamic changes would be good indicators of potential anaplastic transformation.

© 2010 Académie des sciences. Published by Elsevier Masson SAS. All rights reserved.

## R É S U M É

La prise en charge thérapeutique des gliomes de grade II OMS constitue un enjeu important lié à la grande dispersion de leur délai de transformation anaplasique. À ce jour, seule l'augmentation progressive de leur volume, objectivée sur des IRM successives, permet de surveiller cette évolution inéluctable. La spectroscopie multinucléaire et l'imagerie de perfusion in vivo donnent cependant accès aux phénomènes métaboliques qui sous-tendent ces modifications morphologiques. Nous proposons un modèle mathématique simple du métabolisme et de l'hémodynamique des gliomes, basé sur des modèles physiologiques que nous avons précédemment développés, et incluant ces données. Cela nous permet de suggérer que certains profils spécifiques de modification métabolique et hémodynamique constitueraient de bons indicateurs d'une potentielle évolution anaplasique.

© 2010 Académie des sciences. Publié par Elsevier Masson SAS. Tous droits réservés.

\* Corresponding author.

E-mail address: remy.guillevin@psl.aphp.fr (R. Guillevin).

## 1. Introduction

Intracerebral gliomas are the most frequent primary brain tumors. WHO grade II gliomas although considered “low grade” inexorably evolve into anaplastic transformation with a very poor prognosis. However, delays of this anaplastic transformation are highly variable from one patient to another. In addition, the overall survival may be increased by appropriate therapeutic attitude towards this potential evolution [1]. It is therefore crucial to explore the evolution of these tumors to propose an appropriate management for each patient.

The magnetic resonance spectroscopy ( $^1\text{H}$  MRS and  $^{31}\text{P}$ ) allows noninvasive monitoring of changes in these tumors, measuring concentrations of metabolites such as glucose, creatine, lactate ( $^1\text{H}$  MRS), ATP and phosphocreatine ( $^{31}\text{P}$  MRS) or intracellular pH ( $^{31}\text{P}$  MRS). It is complemented by the measurement of regional cerebral blood flow (rCBF), as calculated from related cerebral blood volume (rCBV) by magnetic resonance imaging (MRI) perfusion. The validity and robustness of the tools used have been demonstrated [2,3]. In contrast, metabolic and hemodynamic changes, involved in the anaplastic transformation, have so far not been a conceptual approach.

To better understand the pathophysiological mechanisms involved, we developed a mathematical model, consisting of a system of nonlinear ordinary differential equations. This model, based on existing physiological models [4,5], includes the major variables measured by MRS and perfusion MRI. This model takes into account the high variability of regional blood flow and lactate measured which were difficult to explain coherently. In particular, it did not seem obvious that lactate, which we demonstrated as an early marker of metabolic changes of tumor evolution [2], has very different values, and sometimes non-monotonic evolution. Taking into account intracellular pH and rCBF by the model of lactate, allows us to have a mathematic simulation of the high dispersion of results obtained from MRS and perfusion MRI with neither recourse to the hypothesis of capillary recruiting highly unlikely in WHO grade II gliomas, nor to the capillary proliferation excluded at this stage. This indicates the importance of studying more thoroughly the transport of lactate across the blood-brain barrier and the membranes of tumor cells.

Overall, the model allows a mathematic simulation of pathophysiological mechanisms as part of a subdivision of the tumors we used as a working tool. This provides important perspectives for understanding the pathogenesis of gliomas, which is complex.

Finally, beyond the limits of the model and the short-term outlook for refining the modeling of brain tumor metabolism directly related to the introduction of new techniques of MRS, we discuss possible links between modeling and individualized monitoring of patients with LGG.

## 2. Method

### 2.1. Patient and method

#### 2.1.1. Patients

This was a prospective study over a period of seven months (January 2009–June 2009) for the recruitment of

patients with glioma of supratentorial hemispheric, low grade.

#### 2.1.2. Inclusion criteria

The inclusion criteria were:

- patient with glioma grade II histologically proven (biopsy or surgery);
- no cancer or steroid treatment before imaging.

#### 2.1.3. Exclusion criteria

The exclusion criteria were:

- age less than 8 years;
- chemotherapy, radiotherapy or surgery before inclusion;
- glioma grade other than grade II;
- contra-indications for MRI.

### 2.2. Image analysis

All patients had a magnetic resonance examination using the same protocol from a Signa HDX 3Tesla imager (GE Healthcare, Milwaukee, WI, USA). The conventional anatomical imaging sequence included a coronal FSE sequence T2-weighted (TR/TE = 3650/85, 240 mm FOV, 320 × 320 matrix), axial FLAIR sequence T2-weighted (TR/TE / TI = 10,000/160/2200 ms, 250 mm FOV, 256 × 192 matrix), a volume FSPGR IR T1-weighted before injection (fast spoiled gradient recalled sequence IR FSPGR, TR/TE = 6.3/2.8 ms, 10 flip angle, 280 mm FOV, 256 × 256 matrix), axial FSE sequence T1-weighted post-gadolinium (TR/TE = 500/20, 240 mm FOV, 512 × 256 matrix) and coronal FSE sequence T1-weighted post-gadolinium (TR/TE = 500/20, 240 mm FOV, 512 × 224 matrix).

Multinuclear MRS requires an additional RF channel adapted to each frequency nuclei studied ( $w^{31}\text{P} = 17.2 \text{ MHz/T}$ ,  $w^1\text{H} = 42.6 \text{ MHz/T}$ ) and a dual core proton-phosphorus. In this study, multinuclear MRS was performed using a Dual Quad antenna  $^1\text{H}/^{31}\text{P}$  (General Electric Healthcare, Milwaukee, Wisconsin, USA) and an amplifier chain phosphorus. All SRM acquisitions were performed before injection of gadolinium from the same PRESS sequence (Point Resolved Single voxel Spectroscopy) for  $^1\text{H}$  MRS with a TR 1500 ms, two different TE 35 and 144 ms, and 128 scans. For  $^{31}\text{P}$  MRS, FID sequence with TR 4000 ms, TE < ms, and 184 scans were performed. Anatomically axial FLAIR T2 sequence was used to position the voxel for MRS  $^1\text{H}$  and  $^{31}\text{P}$ . For  $^1\text{H}$  MRS, five voxels were positioned, each of 3 to 8  $\text{cm}^3$  (depending on the size of the lesion): (1) in the center of the tumor; (2) peritumoral; (3) border tumor/“healthy” parenchyma; (4) ipsi lateral “healthy” parenchyma; and (5) contralateral “healthy” parenchyma. For each tumor, only the  $^1\text{H}$  spectrum with the most pejorative parameters such as an increase of ratio Choline/NAA and the presence of resonances of lactate and free lipids were used for analysis. Thus, the voxel for MRS acquisition  $^{31}\text{P}$  was positioned on the same location as the voxel  $^1\text{H}$  with the most pejorative settings and on the contralateral “healthy” parenchyma. All spectroscopic data have been processed with the Spectral Analysis General Electric software (SAGE). For accurate

quantification, Cr resonance from the contralateral side was used as reference. Free lipids (0.9 and 1.3 ppm) were assessed at short echo time and lactate (1.33 ppm) at long echo time. Intracellular pH<sub>i</sub> was calculated from the gap between PCr phosphocreatine and inorganic phosphate Pi-resonances [6].

$$pH_i = 6.75 + \log \left[ \frac{-3.27 + \delta Pi}{-\delta Pi + 5.69} \right]$$

Dynamic contrast agent-enhanced T2\*-weighted gradient-echo echoplanar images (TR/TE = 500/54, 40 sections with a section thickness of 5 mm, FOV of 240 mm, matrix of 128 × 128 and flip angle of 30) were acquired during the first pass of a standard dose (0.1 mmol/Kg) bolus of gadoteric acid (Dotarem, Guerbet, France). Data processing was performed by using the functool software under Advantage Window. ROIs were targeted in the most pejorative location determined from the rCBV color map. Care was taken to avoid the averaging of volume with blood vessels and to minimize confounding factors in analysis of rCBV. The size of ROIs was kept constant. The measurements of rCBV were made by a neuroradiologist experienced with perfusion technique data acquisition at our institution. Then, the position of maximum rCBV ROI was compared to that of the voxel showing the most significant spectral changes.

### 2.3. Model description

The model is based on models of brain energy metabolism previously developed by one of us and colleagues [4,5]. The two state variables of the model of Aubert et al. [5] were the intracapillary and extracellular (interstitial) concentrations of lactate. Our approach is similar, but the state variables of our model are the intracapillary and intracellular concentrations of lactate ( $LAC_c$  and  $LAC_i$ , respectively; concentration of species X is written X rather than [X]). Furthermore, our model takes into account the following parameters and variables (Fig. 1): (i) the cellular production of lactate due to

glycolysis,  $J_1$ ; (ii) the flow of lactate transport from cells towards capillaries,  $J_2$ ; (iii) a flow referred to as  $J_3$ , namely the sum of the consumption of lactate by mitochondria, via its transformation to pyruvate catalyzed by lactate dehydrogenase (LDH), and diffusion of lactate from the ROI towards neighboring regions, via gap-junctions [7] or via the interstitial milieu; (iv) cerebral blood flow (CBF); and (v) intracellular pH, ( $pH_i = -\log H_i^+$ ). Concentrations of lactate and  $H^+$  are expressed in mM and M, respectively. The volumes and flows are expressed per unit tissue volume:  $V_c$  and  $V_i$  are respectively the dimensionless capillary and intracellular volume fractions; similarly, CBF is expressed in  $s^{-1}$ . Lactate flows are expressed in  $mM s^{-1}$ .

The metabolic balance equations of intracellular and intracapillary lactate leads to the following system of differential equations:

$$V_i \frac{dLAC_i}{dt} = J_1 - J_2 - J_3 \quad (1)$$

$$V_c \frac{dLAC_c}{dt} = J_{cap} + J_2 \quad (2)$$

$J_{cap}$  is the contribution of blood flow to the variation of intracapillary lactate, as described below. We set by definition:

$$J = J_1 - J_3 \quad (3)$$

We took into account the effects of intracellular and intracapillary concentrations of  $H^+$  on the transport of lactate by setting:

$$J_2 = T \left( \frac{LAC_i H_i^+}{K_H + LAC_i H_i^+} - \frac{LAC_c H_c^+}{K_H + LAC_c H_c^+} \right) \quad (4)$$

$K_H$  is a parameter expressed in  $mM \times M$ ,  $T$  is the maximum rate of transport. It must be emphasized that  $T$  depends both on the total area of capillary endothelium and the density of lactate-proton cotransport proteins, namely monocarboxylate transporters (MCTs). Formula (4) was obtained from a more general formula for cotransport [8]. The intracellular concentration of protons  $H_i^+$  was measured using  $^{31}P$  MRS, while the intracapillary concentration of protons  $H_c^+$  is considered as constant. In the following, we define the variable  $LACH$  as being the product  $LAC_i H_i^+$ .

The contribution of CBF to the change of  $LAC_c$  is given by balance equation:

$$J_{cap} = CBF \cdot (LAC_a - LAC_v) \quad (5)$$

$LAC_a$  and  $LAC_v$  are the arterial and venous concentrations of lactate, respectively. Based on previous model [5], we obtain:

$$J_{cap} = CBF \cdot LAC_a - CBF \cdot LAC_v = 2 CBF \cdot (LAC_a - LAC_c) \quad (6)$$

A similar equation was proposed by Gjedde for oxygen [9]. It follows from the simple assumption  $LAC_c \approx (LAC_a + LAC_v)/2$ . We have shown that this simple formulation is nearly equivalent to much more complex approaches, based on partial differential equations [10].

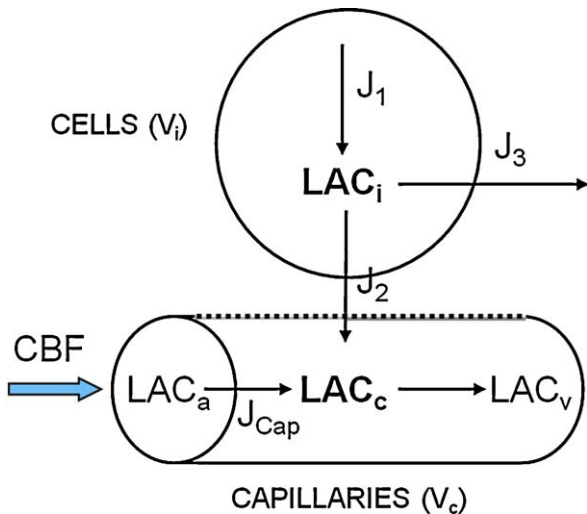


Fig. 1. Description of the mathematical model.

In summary, the system of ordinary differential equations describing the system is written as follows:

$$\begin{aligned} \frac{dLAC_i}{dt} &= \frac{1}{V_i} \left[ J - T \left( \frac{LAC_i H_i^+}{K_H + LAC_i H_i^+} - \frac{LAC_c H_c^+}{K_H + LAC_c H_c^+} \right) \right] \\ \frac{dLAC_c}{dt} &= \frac{1}{V_c} \left[ 2 CBF \cdot (LAC_a - LAC_c) + T \left( \frac{LAC_i H_i^+}{K_H + LAC_i H_i^+} - \frac{LAC_c H_c^+}{K_H + LAC_c H_c^+} \right) \right] \end{aligned} \quad (7)$$

The values of  $V_i$ ,  $V_c$ ,  $H_c^+$ ,  $LAC_a$  and  $K_H$  are provided by the literature (for a discussion: [4,5,9,10]). Data from MRI and MRS provide  $LAC_i$ ,  $H_i^+$  and  $CBF$ . However, it is much more difficult to assign values to  $J$  and  $T$ , which is the major reason for using a model.

### 3. Results

#### 3.1. MRI results

Fifteen patients with grade II WHO gliomas, were included in this study, seven (43.7%) males and eight (56.3%) females. Six patients had oligodendrogliomas, five astrocytomas and four mixed gliomas. All settings MRS and perfusion are summarized in Table 1.

The analysis of the data summarized in Table 1, shows three homogeneous subgroups corresponding to the three spectral groups detailed in the study of Guillevin et al. [2]:

- Class 1: six patients had a marked increase of the ratio PME/PDE due to an increase of PME (PDE were stable), an increase of the ratio Cho/Cr, a stable pH<sub>i</sub>, a resonance of lactate and an increase of rCBV which remained less than 1.7 (Fig. 2);
- Class 2: three patients had a stable ratio of PME/PDE due to a both increase of PME and PDE, a stable ratio of Cho/Cr, a resonance of free lipids, a stable pH<sub>i</sub>, an inconstant resonance of lactate, and an increase of rCBV, which remained still less than 1.7 (Fig. 3);
- Class 3: six patients had an increase of the ratio PME/PDE due to an increase of PME more than the increase of PDE, an increase of ratio Cho/Cr, a resonance of free lipids

associated to a resonance of lactate and an increase of pH<sub>i</sub> (Fig. 4).

#### 3.2. Model results

The programs were written in MATLAB language to solve ODE system (7). Numerical simulations strongly suggest that system (7) has a unique, asymptotically stable steady state (data not shown). However, a full mathematical study of system (7) is beyond the scope of this article: since tumor metabolism can be assumed to be almost constant during data recording, we focused on steady states.

For convenience, we used the following notations:

- $\alpha_F$ : ratio  $CBF/CBF_0$ , where  $CBF_0$  is the normal blood flow; this ratio can be assumed to be the same as rCBF in data;
- $\alpha_J$ : relative increase of  $J$  with respect to reference value  $J_0$ , i.e. ratio  $J/J_0$ ;
- $\alpha_T$ : relative increase of  $T$  with respect to reference value  $T_0$ , i.e. ratio  $T/T_0$ .

Thus, the reference steady state corresponds to  $\alpha_F = \alpha_J = \alpha_T = 1$ . Reference values were obtained from data in normal human and previous model estimations [4,5,8,9].

We addressed a question where the straightforward interpretation of data gives no simple answer: what are the respective contributions of blood flow, lactate transport, and  $J$  on the variations of the  $LACH = LAC_i \cdot H_i^+$  product? On the one hand, the characteristics of Class 3 gliomas, with a marked increase of both  $LACH$  and  $CBF$ , and a significant decrease in  $H_i^+$ , were easy to obtain using the model, by assuming large enough values of  $CBF$  and  $J$  (data not

**Table 1**  
Results of  $^1H$  MRS,  $^{31}P$  MRS and perfusion MRI, for the 15 patients studied.

Patient	Cho/cr	Cho/NAA	Lact/cr	Lip/cr	PME/PDE	pHi	rCBV	rCBF	Class
1	1.98	1.77	0.38	0.8	1.69	7.09	2	3.27	3
2	0.84	1.75	0.96	-	1.52	7.01	0.89	1.7	1
3	2.93	5.87	0.96	2.9	2.25	7.11	2.47	0.87	3
4	4.19	6.99	1.85	0.56	1.87	7.09	2.17	1.56	3
5	2.87	5.13	0.76	1.25	1.26	6.99	1.58	3.73	2
6	1.08	1.89	0.61	1.4	1.11	7.01	1.46	1.73	2
7	1.85	11.58	1.5	-	1.25	6.98	0.36	0.31	1
8	1.55	0.83	1.41	-	0.98	7	0.56	0.74	1
9	2.55	2.55	1.37	-	1.16	6.98	0.36	0.29	1
10	3	4.62	1.28	-	1.48	6.97	1.03	0.68	1
11	1.14	1.78	0.54	1.95	0.87	6.98	1.23	0.94	2
12	2.89	1.72	4.22	3.32	1.51	7.1	1.73	2.51	3
13	2.28	3.55	2.47	3.28	1.72	7.1	1.85	2.16	3
14	4.79	4.6	7.53	1.07	2.15	7.08	2.19	4.25	3
15	2.23	1.54	1.16	-	1.24	7.02	1.07	1.28	1

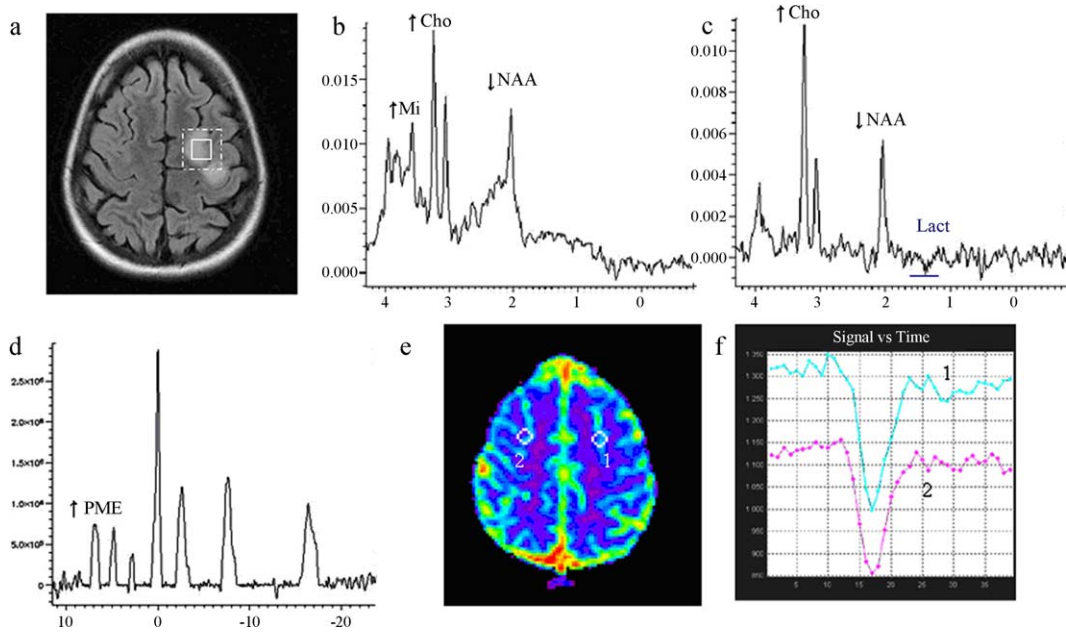


Fig. 2. Imaging of low-grade glioma Class 1. (a) Location of proton voxel and phosphorus voxel on the left frontoparietal lesion, T2 FLAIR sequence. (b)  $^1\text{H}$  MRS short TE showing an increase of choline and a decrease of NAA. (c)  $^1\text{H}$  MRS long TE showing discrete onset of lactate. (d)  $^{31}\text{P}$  MRS, an increase of PMEs,  $\Delta\text{pPi} = 4.79$ ,  $\text{pHi} = 6.98$ . (e) Perfusion MRI, a mapping of cerebral blood volume (rCBV), and (f) Perfusion MRI, first pass curves: hypoperfusion with  $\text{rCBV} = 0.8$ .

shown). On the other hand, the hemodynamics and metabolism of Class 1 and Class 2 gliomas were more difficult to explain. In particular, a negative correlation was observed between rCBF and the *LACH* product in Class 1, as

displayed in Fig. 5. This somewhat paradoxical result was explored by calculating model steady states: *LACH* is plotted vs.  $\alpha_F$  (i.e., rCBF) in Fig. 6 for various values of *J* and *T*. It can be seen that assuming constant *J* and *T* values

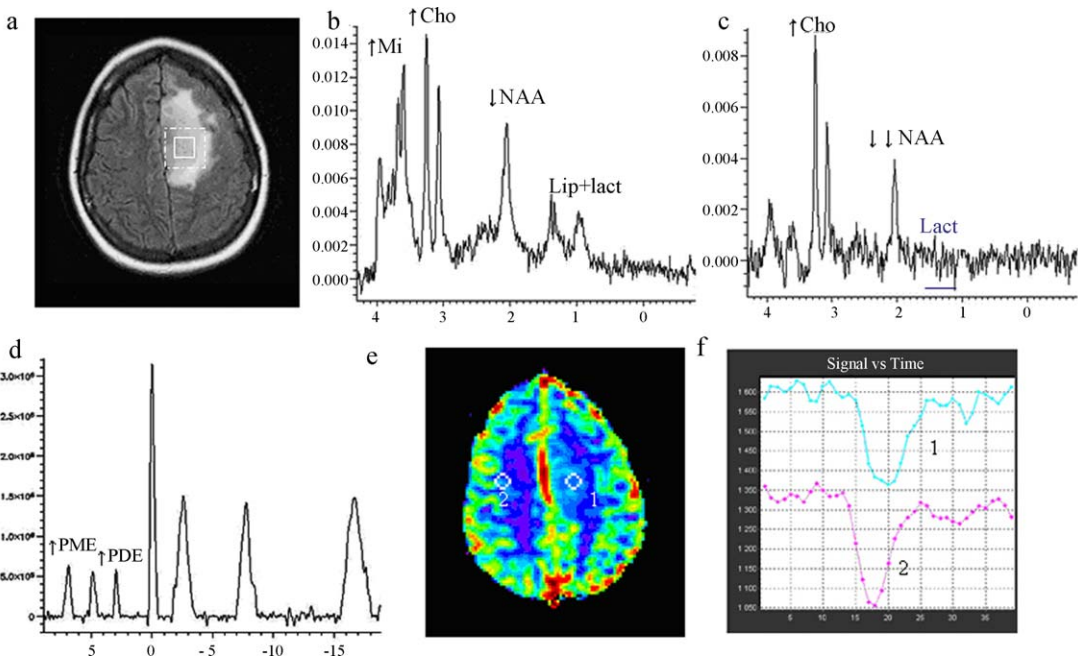
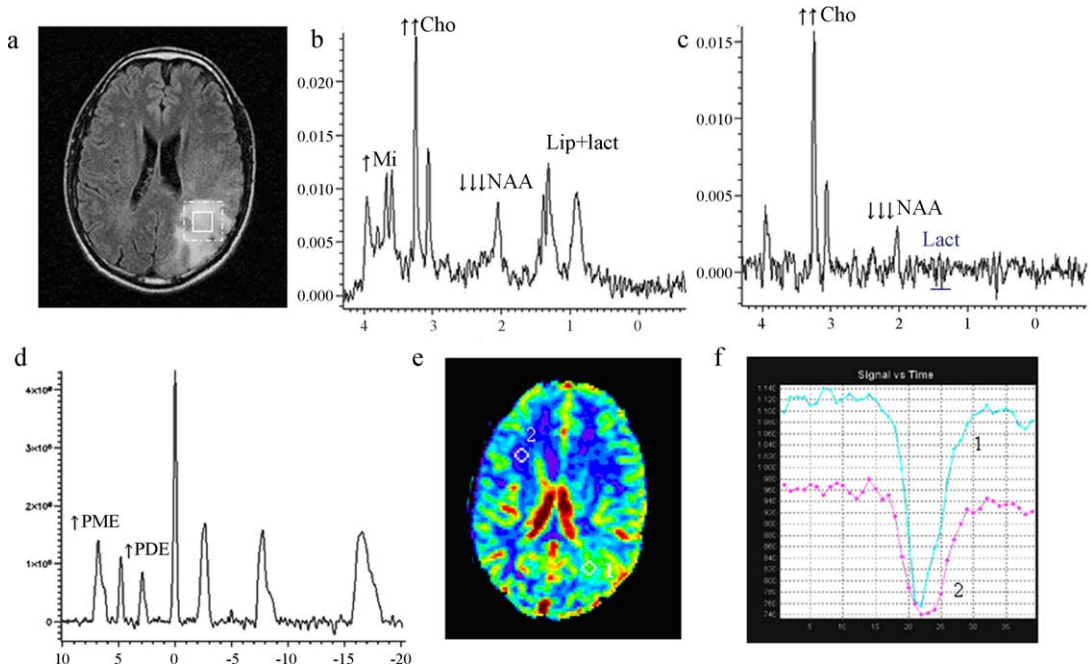


Fig. 3. Imaging of low-grade glioma, Class 2. (a) Location of proton voxel and phosphorus voxel on the left frontoparietal lesion, T2 FLAIR sequence. (b)  $^1\text{H}$  MRS short TE showing an increase of choline, a decrease of NAA and presence of lipid/lactate. (c)  $^1\text{H}$  MRS long TE, presence of lactate. (d)  $^{31}\text{P}$  MRS, an increase of PMEs,  $\Delta\text{pPi} = 4.81$ ,  $\text{pHi} = 6.99$ . (e) Perfusion MRI, a mapping of cerebral blood volume (rCBV), and (f) Perfusion MRI, first pass curves: hypoperfusion with  $\text{rCBV} = 1.2$ .





**Fig. 4.** Imaging of low-grade glioma Class 3. (a) Location of proton voxel and phosphorus voxel on the left frontal lesion, T2 FLAIR sequence. (b) <sup>1</sup>H MRS short TE showing an increase of choline, a dramatic decrease of NAA and large presence of lipid/lactate. (c) <sup>1</sup>H MRS long TE, presence of lactate. (d) <sup>31</sup>P MRS, an increase of PMEs, deltaPi = 4.92, pHi = 7.08. (e) Perfusion MRI, a mapping of cerebral blood volume (rCBV), and (f) Perfusion MRI, first pass curves: hyperperfusion with rCBV = 2.23.

cannot explain MR data of Fig. 5: Strikingly, the LACH product varies only very slightly for  $\alpha_F$  varying from 0.7 to 1.7, which does not match MR data. Moreover, assuming that  $T$  is equal to its reference value (Dark blue curve) results in a poor agreement with MR data. In order to further discuss these points, some typical model results are displayed in Table 2.

Case 1 indicates that, when CBF is not increased, an increase of  $J$  alone can easily explain the observed data. However, when CBF is increased (cases 2–5), the pathophysiological mechanisms cannot be explained in a

straightforward way. First, we will assume that the increase in  $J$  in cases 2–5 is equal or greater than the increase in  $J$  in case 1, which seems a reasonable assumption since increased CBF seems linked to increased tumor mass or tumor metabolism (see MRI results). According to case 2, an increase in  $J$  equal or similar to

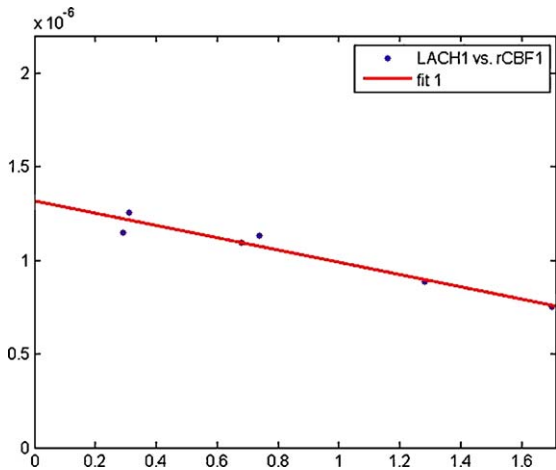


**Fig. 5.** Regression line “LACH vs. rCBF” for Class 1 gliomas ( $r = 0.97$ ,  $\alpha < 0.05$ ).

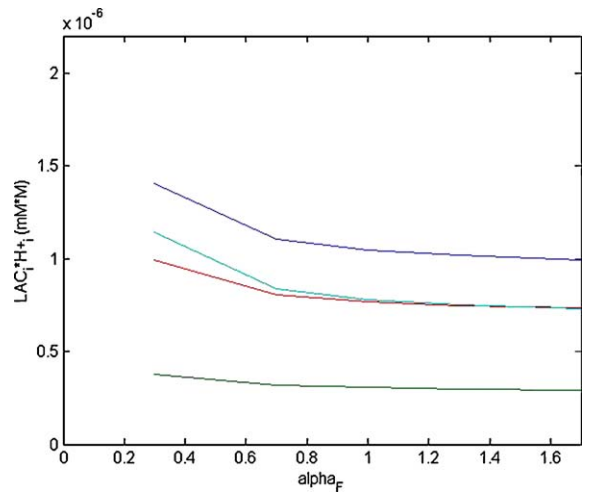


**Fig. 6.** Model results for Class 1 gliomas: LACH is plotted vs.  $\alpha_F$  (i.e., rCBF). Parameter values are:  $CBF_0 = 0.01 \text{ s}^{-1}$ ,  $J_0 = 0.001 \text{ mM s}^{-1}$ ,  $T_0 = 0.0061 \text{ mM s}^{-1}$ ,  $K_H = 3.5 \cdot 10^{-7} \text{ mM.M}$ ,  $H_c^+ = 10^{-7.35} \text{ M}$ , as in [4]. Since  $H_i^+$  varies very slightly amongst Class 1 gliomas, we set  $H_i^+ = 10^{-7} \text{ M}$  according to <sup>31</sup>P MRS data. (Dark blue)  $\alpha_j = 4.2$ ,  $\alpha_T = 1.0$ ; (Green)  $\alpha_j = 4.2$ ,  $\alpha_T = 1.7$ ; (Red)  $\alpha_j = 4.2$ ,  $\alpha_T = 1.1$ ; (Cyan)  $\alpha_j = 6.4$ ,  $\alpha_T = 1.7$ .

**Table 2**  
Some simulation results for Class 1 gliomas.

Simulation case	$\alpha_F$	$\alpha_J$	$\alpha_T$	$LACH = LAC_i \cdot H_i^+$	Agreement with MR data
				(mM.M)	LACH vs. rCBF
1	1.0	4.2	1.0	$1.05 \cdot 10^{-6}$	Yes
2	1.7	4.2	1.0	$9.95 \cdot 10^{-7}$	No ( <i>LACH</i> too high)
3	1.7	4.2	1.7	$2.94 \cdot 10^{-7}$	No ( <i>LACH</i> too low)
4	1.7	4.2	1.1	$7.34 \cdot 10^{-7}$	Yes
5	1.7	6.4	1.7	$7.30 \cdot 10^{-7}$	Yes

the increase in case 1 cannot fit clinical data; this indicates that in case 2 the increase in CBF, although resulting in a lactate ‘washout’, is not sufficient to explain the decrease in *LACH*.

It can be noted that in case 2, CBF is increased but *T* remains constant, which means that neither capillary recruitment nor increase in MCTs density occurs; CBF increase is due solely to an increase of blood velocity in the capillaries. An alternative hypothesis is that *CBF* and *T* are increased by the same factor (case 3), due to, for instance, the recruitment of capillaries or proliferation of new blood vessels; however, in this case the *LACH* product is too low.

Thus it was necessary to refine the assumptions. We could indeed get for rCBF = 1.7, a value consistent with the regression line “LACH vs. rCBF” for Class 1, in each of the following situations:

- case 4, which consists in an increase of CBF with only a moderate increase of *T*. MRI data demonstrated that rCBV was only slightly increased or declined, which seemed consistent with this hypothesis. However, the major determinant of rCBV is venous volume, not capillary volume, so it is somewhat risky to relate it to capillary recruitment or proliferation;
- case 5, in which we assumed that the increase of CBF is accompanied by a parallel increase in *T* and a major increase of *J*.

In conclusion, the decrease of *LACH* when rCBF increases, observed in Class 1, cannot be achieved by an increased of CBF due solely to the increase of blood flow velocity. It is necessary, whatever the assumptions about *J*, to suppose an increase of *T*. The increase of the parameter *T* may correspond to: (i) an increase of the area of the blood-brain barrier, due to the recruitment and/or proliferation of capillaries; (ii) an increase of lactate transport by a change of the density or the kinetic properties of lactate- $H^+$  carriers (MCTs).

However, hypothesis (i) could probably be discarded because the WHO grade II glioma excludes the presence of capillary proliferation, and capillary recruitment does not seem to be a major mechanism of CBF regulation [11]. Moreover, if we assumed an increase of *J* (which is not necessary, as we have seen), knowing that  $J = J_1 - J_3$ , this increase may be due to an increase of glycolysis  $J_1$ , but also to a decrease of  $J_3$  which corresponds to the diffusion of lactate towards the neighboring regions and/or to the consumption of lactate by neurons via lactate shuttle [12].

Thus, the model provided preliminary arguments to explain the observations of MRS and MRI. For example, it

suggested the potential role of changes of MCTs, which play a major role in brain energy metabolism [12].

#### 4. Discussion

The WHO grade II gliomas exhibit characteristics affecting their therapeutic management [13]. Their delay of change in tumor grade is highly variable from one subject to another [14]. To date, only clinical events or continuous observations of the growth of the tumor volume on repeated examinations can evoke a change in tumor grade. It is therefore necessary to repeat the MRI at regular intervals to obtain a predictive parameter, namely the growth of average diameter [15]. However, in addition to requiring regular inspections, this approach is purely morphological and has the disadvantage of revealing the consequences of changes of tumor biometabolism, which occur upstream of tumor growth and of degeneration of the lesion. Indeed, switching the metabolism of grade II glioma to a much closer metabolism to that of high grade gliomas occurs very early during the natural history of gliomas [16]. It is therefore obvious that volume growth and metabolic changes are not synchronous and that metabolic changes precede the growth of tumor volume. Therefore it seemed important to attempt an investigation of these changes in tumor metabolism, using a biomathematical model with simulations from metabolic data, collected in vivo by magnetic resonance. For the first time we propose a model combining the parameters of  $^1H$  MRS,  $^{31}P$  MRS and the MRI perfusion.

Indeed, previous studies conducted in  $^1H$  MRS, had not demonstrated the existence of discriminate factors between different subgroups of grade II, probably because they were conducted from inhomogeneous population in tumor grade [17,18]. Recently, we conducted a study [2] from a homogeneous population of WHO grade II gliomas. This study revealed three different spectral profiles  $^1H$  according to the classes of Ki-67, marking tumor antigen considered a marker of tumor aggressiveness underlying. In this population of grade 2, the appearance of a resonance of lactate, which reflects an abnormally high concentration of lactate, appeared to be predictive of a Ki-67 greater than 4%. The question we might ask is lactate could be considered as a marker of tumor aggressiveness. In addition, the detection of lactate was inconstant in the third group of patients with Ki-67 greater than 8%, reflecting a decrease of lactate concentration. The second question we can ask is, what is the mechanism involved in the decrease in lactate. Factors that may play a major role are particularly the regional blood flow, the values of pH, lactate transport which run via the MCT, carriers lactate- $H^+$  [12].

To better understand the pathophysiological mechanisms involved, we constructed a mathematical model consisting of a system of nonlinear ordinary differential equations. We implemented this model using in vivo data from multinuclear MRS ( $^1H/^{31}P$ ) and perfusion MRI. This model is based on existing physiological models [4,5], and its variables or parameters are mostly measured by MRS and MRI perfusion. We tried to explain the great variability

of regional blood flow, lactate and pHi, which were difficult to explain coherently.

The implementation of the model with the data from our study allows identification of different subgroups based on lactate, pHi and data from MRS perfusion. Thus, gliomas expressing lactate and an increase in CBF, also show an increase in pHi. These results are consistent with the experimental study of Hubesch et al. [19], which showed that despite a potential increase in glycolysis, the pHi of tumor cells is likely to increase due to alterations of membrane transporters proton/bicarbonate.

On the other hand, it seemed paradoxical that lactate, which we have shown that it would be a very early marker of changes of tumor metabolism [2], has values very different, and sometimes a non-monotonic evolution. Taken into account intracellular pH and rCBF by the model of lactate, allows one to have a mathematic simulation of the high dispersion of results obtained from MRS and perfusion MRI without nether recourse to the hypothesis of capillary recruiting highly unlikely in WHO grade II gliomas, nor to the capillary proliferation excluded at this stage. However, our results strongly suggest changes in the transport of lactate across the blood-brain and the membranes of tumor cells. This hypothesis can be in relation with the resonance of free lipids observed in lesions showing no detectable lactate resonance. It is consistent with recent data from the literature, which suggest qualitative or quantitative changes of MCTs in glial tumors.

This mathematical modeling from in vivo data allows considering to design a longitudinal study of grade 2 gliomas, in order to objectify the predictive power of that model.

#### Conflict of interest statement

None.

#### References

- [1] M.S. Berger, A.V. Deliganis, J. Dobbins, G.E. Keles, The effect of extent of resection on recurrence in patients with low-grade cerebral hemisphere gliomas, *Cancer* 6 (1994) 1784–1791.

- [2] R. Guillevin, C. Menuel, H. Duffau, M. Kujas, L. Capelle, A. Aubert, S. Taillibert, A. Idbah, J. Pallud, G. Demarco, R. Costalat, K. Hoang-Xuan, J. Chiras, J.N. Vallee, Proton magnetic resonance spectroscopy predicts proliferative activity in diffuse low-grade gliomas, *J. Neurooncol.* 2007.
- [3] M. Law, S. Oh, G. Johnson, J.S. Babb, D. Zagzag, J. Golfinos, et al., Perfusion magnetic resonance imaging predicts patient outcome as an adjunct to histopathology: a second reference standard in the surgical and nonsurgical treatment of low-grade gliomas, *Neurosurgery* 58 (6) (2006) 1099–1107 (discussion 1099–107).
- [4] A. Aubert, R. Costalat, Interaction between astrocytes and neurons studied using a mathematical model of compartmentalized energy metabolism, *J. Cereb. Blood Flow Metab.* 25 (11) (2005) 1476–1490.
- [5] A. Aubert, R. Costalat, P.J. Magistretti, L. Pellerin, Brain lactate kinetics: modeling evidence for neuronal lactate uptake upon activation, *Proc. Natl Acad. Sci. U S A* 102 (45) (2005) 16448–16453.
- [6] O.A. Petroff, J.W. Prichard, K.L. Behar, J.R. Alger, J.A. den Hollander, R.G. Shulman, Cerebral intracellular pH by <sup>31</sup>P nuclear magnetic resonance spectroscopy, *Neurology* 35 (6) (1985) 781–788.
- [7] N. Rouach, A. Koulakoff, V. Abudara, K. Willecke, C. Giaume, Astroglial metabolic networks sustain hippocampal synaptic transmission, *Science* 322 (2008) 1551–1555.
- [8] J. Keener, J. Sneyd, *Mathematical physiology*, Springer-Verlag, New-York, 1998, p. 48.
- [9] A. Gjedde, *Cerebrovascular disease*, H.H. Batjer (Ed.), Lippincott-Raven, Philadelphia, 1997, pp. 23–40.
- [10] R. Valabregue, A. Aubert, J. Burger, J. Bittoun, R. Costalat, Relation between cerebral blood flow and metabolism explained by a model of oxygen exchange, *J. Cereb. Blood Flow Metab.* 23 (5) (2003) 536–545.
- [11] R.B. Buxton, *Introduction to functional magnetic resonance imaging*, Cambridge University Press, 2002.
- [12] L. Pellerin, Brain energetics (thought needs food), *Curr. Opin. Clin. Nutr. Metab. Care* 11 (6) (2008) 701–705.
- [13] H. Duffau, New concepts in surgery of WHO grade II gliomas: functional brain mapping, connectionism and plasticity: a review, *J. Neurooncol.* 1 (2006) 77–115.
- [14] R. Durmaz, M. Vural, E. Isildi, E. Cosan, E. Ozkara, C. Bal, et al., Efficacy of prognostic factors on survival in patients with low-grade glioma, *Turk. Neurosurg.* 4 (2008) 336–344.
- [15] E. Mandonnet, J.Y. Delattre, M.L. Tanguy, K.R. Swanson, A.F. Carpentier, H. Duffau, et al., Continuous growth of mean tumor diameter in a subset of grade II gliomas, *Ann. Neurol.* 4 (2003) 524–528.
- [16] F. Lamari, R. La Schiazza, R. Guillevin, B. Hainque, M.J. Foglietti, J.L. Beaudeau, et al., Biochemical exploration of energetic metabolism and oxidative stress in low-grade gliomas: central and peripheral tumor tissue analysis, *Ann. Biol. Clin. (Paris)* 66 (2) (2008) 143–150.
- [17] M. Castillo, J.K. Smith, L. Kwock, Correlation of myo-inositol levels and grading of cerebral astrocytomas, *AJNR Am. J. Neuroradiol.* 9 (2000) 1645–1649.
- [18] D. Yang, Y. Korogi, T. Sugahara, M. Kitajima, Y. Shigematsu, L. Liang, et al., Cerebral gliomas: prospective comparison of multivoxel 2D chemical-shift imaging proton MR spectroscopy, echoplanar perfusion and diffusion-weighted MRI, *Neuroradiology* 8 (2002) 656–666.
- [19] B. Hubesch, D. Sappey-Mariniere, K. Roth, D.J. Meyerhoff, G.B. Matson, M.W. Weiner, P-31 MR spectroscopy of normal human brain and brain tumors, *Radiology* 174 (2) (1990) 401–409.